



# Room-temperature magnetoresistance of nanocrystalline Ni metal with various grain sizes

V. A. Isnaini<sup>1,5</sup>, T. Kolonits<sup>2,5</sup> , Zs. Czirány<sup>2</sup> , J. Gubicza<sup>3</sup> , S. Zsurzsa<sup>1,4</sup>,  
L. K. Varga<sup>1</sup> , E. Tóth-Kádár<sup>1</sup>, L. Pogány<sup>1</sup>, L. Péter<sup>1</sup> , I. Bakonyi<sup>1,a</sup>

<sup>1</sup> Wigner Research Centre for Physics, Hungarian Academy of Sciences, Konkoly-Thege út 29-33, Budapest 1121, Hungary

<sup>2</sup> Centre for Energy Research, Institute for Technical Physics and Materials Science, Hungarian Academy of Sciences, Konkoly-Thege út 29-33, Budapest 1121, Hungary

<sup>3</sup> Department of Materials Physics, Eötvös Loránd University, Pázmány Péter sétány 1/A, Budapest 1117, Hungary

<sup>4</sup> Present Address: Infineon Technologies Cegléd Kft., Cegléd, Hungary

<sup>5</sup> Eötvös University, Doctoral School of Physics, Budapest, Hungary

Received: 6 July 2019 / Accepted: 20 October 2019

© The Author(s) 2020

**Abstract** The room-temperature magnetoresistance (MR) characteristics of nanocrystalline (nc) Ni metal with various grain sizes (between 30 and 100 nm) are investigated in this work for the first time. The nc-Ni foils were produced by electrodeposition and the results are compared with data measured on coarse-grained (bulk) pure Ni metal samples prepared by cold-rolling and annealing. The  $MR(H)$  curves measured in magnetic fields up to  $H = 9$  kOe are analyzed in detail to determine the anisotropic magnetoresistance (AMR) ratio. The magnitude of the AMR ratio was found to be around 2.5% for bulk Ni and in the range from about 2 to 2.5% for the nc-Ni samples, the latter data not exhibiting a systematic dependence on the grain size. On the other hand, the field-induced resistivity anisotropy splitting  $\Delta\rho_{AMR}$  in the magnetically saturated state of the nc-Ni series was found to be proportional to the zero-field resistivity of the same samples with different grain sizes. The slope of this proportionality relation provided an AMR ratio of 2.4% for all nc-Ni samples, matching well the value for the bulk Ni samples. Thus, the AMR ratio for polycrystalline Ni metal seems to be fairly independent of the microstructural features. This also means that the AMR ratio is an inherent characteristic of the Ni metal matrix and it remains the same even if the matrix resistivity changes (e.g., by introducing grain boundaries) without noticeably modifying the electronic density of states at least in the vicinity of the Fermi level.

## 1 Introduction

Spintronic and magnonic materials are two important classes of advanced materials and their study is at the forefront of materials science. Such materials are typically composed of nanoscale ferromagnetic entities separated by a non-magnetic metal, an air gap or another ferromagnetic metal of different magnetic characteristics. The interest in these materials arises, on the one hand, due to the already existing applications, e.g., in spintronics devices

<sup>a</sup> e-mail: [bakonyi.imre@wigner.mta.hu](mailto:bakonyi.imre@wigner.mta.hu)

such as the read heads of magnetic hard disk drives based on the giant magnetoresistance effect [1, 2]. The ongoing demand for improving these existing applications necessitates further study of nanoscale magnetic heterostructures. On the other hand, there are further prospective technological applications of such structures, e.g., information storage in magnonic crystals [3, 4].

Since the ferromagnetic elements Fe, Co and Ni as well as their alloys with each other often appear as basic ingredients of these magnetic nanostructures, it is important to have a reliable detailed knowledge of their electrical transport and magnetic properties since it appears from the literature that available data are not always satisfactorily accurate. This justifies revisiting, e.g., the zero-field electrical resistivity and the magnetoresistance (MR) characteristics of these ferromagnets both in the bulk state and in their various nanostructured forms.

In the present work, the room-temperature MR characteristics of Ni metal in the nanocrystalline (nc) state are investigated for the first time. The investigated nc-Ni foils were produced by electrodeposition and the results will be compared with data measured on coarse-grained (bulk) pure Ni metal samples prepared by cold-rolling and annealing.

For the electrodeposited Ni foils, the grain size could be varied by the deposition parameters between about 30 and 100 nm, and thus the possible influence of grain size on the electrical transport parameters could be investigated. This is of interest since in the nanocrystalline state, the presence of a large amount of lattice defects such as grain boundaries represent excess scattering centers for the conduction electrons carrying the current and this leads finally to an increase of the zero-field resistivity [5]. This was, indeed, often observed for nc-Ni as summarized in Ref. [6] in which we have analyzed the grain-size dependence of the zero-field resistivity ( $\rho_0$ ) of the current electrodeposited nc-Ni samples together with all previously reported relevant data to extract the specific grain-boundary resistivity of Ni metal.

Although Madduri and Kaul [7] investigated in detail the temperature and field dependence of the resistivity of electrodeposited nc-Ni samples, they have measured the transverse magnetoresistance component only. Thus, the anisotropic magnetoresistance (AMR) could not be derived from their measurements since for deducing the AMR, the longitudinal magnetoresistance should also be measured. Therefore, in the present work the  $MR(H)$  curves were measured on nc-Ni samples with two orientations of the magnetic field with respect to the current: field parallel to the current flow (longitudinal MR = LMR) and field perpendicular to the current flow (transverse MR = TMR). From the saturation value of the longitudinal and transverse MR components, obtained by extrapolation from the magnetically saturated (single-domain) state to  $H = 0$ , the AMR ratio [8–13] was determined. The main aim of the present study was to reveal whether the grain size has an influence on the AMR of a ferromagnetic metal.

This contribution is organized as follows. In Sect. 2, the investigated Ni samples and the electrical transport measurement technique will be presented. The experimental results for the room-temperature MR behavior of the samples studied are described in Sect. 3, where they are also discussed in comparison with previous reports on Ni metal, either in bulk, thin film or nanocrystalline form. In Sect. 4, the correlation between the zero-field resistivity data and the saturation value of the magnetic-field-induced resistivity change is discussed. A summary of the present results will be given in Sect. 5.

## 2 Experimental

### 2.1 Samples investigated

The results of electrical transport measurements to be presented here were obtained on the same metallurgically processed and electrodeposited pure Ni metal foil samples for which we have recently reported room-temperature zero-field resistivity data [6]. Therefore, only a brief description and characterization of these samples will be given here.

- (1) Metallurgically processed Ni foils were prepared by cold rolling and annealing ingots from two different sources. The samples prepared in this manner included the following Ni foils: sample #B5 prepared from electrolytic grade Ni and sample #Ni(99.99+%) prepared from a high-purity ingot. An additional Ni sample was also included in the electrical transport studies: sample #GF-Ni(50  $\mu\text{m}$ ) purchased from Goodfellow Company in the form of a foil with a thickness of 50  $\mu\text{m}$ . The structural characterization of sample #B5 revealed [6] that this Ni foil sample can be considered as representing the bulk state of Ni (it can also be termed as microcrystalline ( $\mu\text{c}$ ) Ni since it exhibits grain sizes in the micrometer range). Although no structural study was carried out for the two other above mentioned Ni foil samples (#Ni(99.99+%) and #GF-Ni(50  $\mu\text{m}$ )), they should exhibit fairly similar structural features as sample #B5, i.e., they can also be considered as representing bulk Ni. This is further supported by the fact that the room-temperature zero-field resistivity of all these samples was in good agreement with that of bulk Ni [6].
- (2) Electrodeposition (ED) was used to prepare about 20  $\mu\text{m}$  thick nc-Ni foils with grain sizes ranging from 30 to 100 nm. The metallic substrates were removed from the nc-Ni samples by mechanical stripping and/or electrochemical etching. A sample set denoted here as ED Ni series is identical with those electrodeposited Ni samples for which a detailed structural characterization was described in Refs. [14] and [15] and their zero-field resistivity data were reported in Ref. [6]. Two other electrodeposited Ni samples (sample #B2 and #Ni(TKE)) prepared earlier under different conditions were also investigated and structurally characterized in Ref. [6] and they will also be included in the present MR study.

According to the chemical analysis reported in Ref. [6], neither metallic, nor non-metallic impurities could be detected up to a level of about 0.1 at.% in most of these investigated Ni foil samples, apart from some C and O contamination, very probably on the surface of the foils only since these elements could be detected roughly in the same amount for each sample even for the metallurgically processed ones. Two of the ED Ni series samples, however, contained about 3 at.% Co due to the Co impurity in the chemicals used for the electrodeposition of these two particular samples. Whereas it was pointed out in Ref. [6] that such an amount of Co impurity has a negligible influence only on the room-temperature zero-field resistivity of Ni metal, it can cause a significant increase of the AMR of Ni metal [12]. Therefore, these two Co-containing nc-Ni samples will be treated separately from the pure nc-Ni samples.

### 2.2 Electrical transport measurements

For the electrical transport measurements, a rectangular strip of about 1–2 mm wide and about 5–20 mm long was cut from the Ni foils.

The magnetoresistance was measured with a four-point-in-line probe with flat gold-coated spring contacts at room temperature. The measurements were performed with both the current

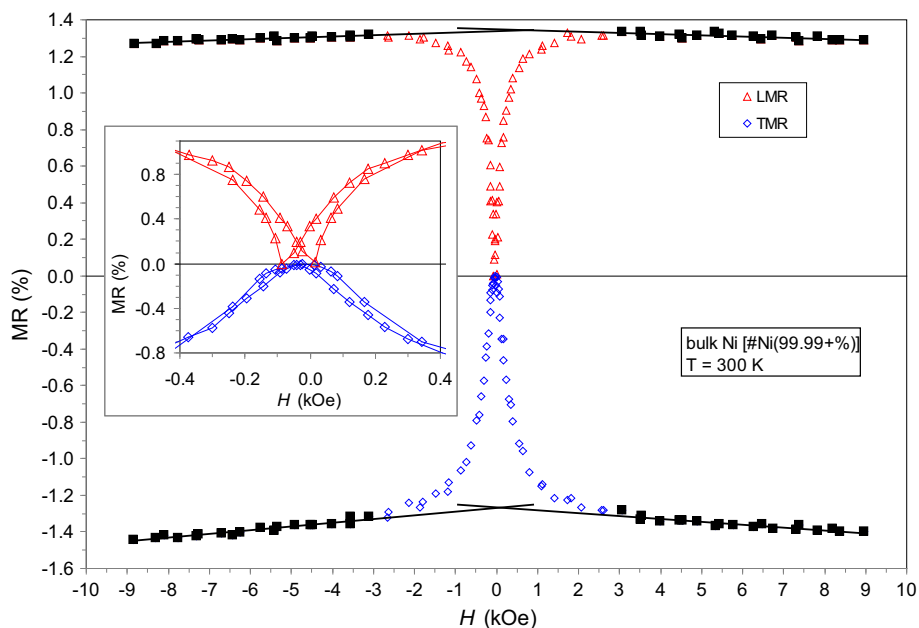


**Fig. 1** Room-temperature longitudinal (LMR) and transverse (TMR)  $MR(H)$  curves for the bulk Ni foil sample #Ni(99.99+%). The solid squares over the high-field ( $|H| \geq 3$  kOe) data points indicate data used for a linear fitting and the fit is also indicated (thick solid line). The inset shows a magnified view around zero magnetic field to demonstrate that by the densely measured points around  $H = 0$ , the real maximum and minimum resistivity values were captured. The magnified inset also allows revealing the hysteretic behavior of the magnetoresistance, analogous to the magnetic hysteresis

and the magnetic field being applied in the foil plane. The  $MR(H)$  curves were measured in both the longitudinal and transverse configurations as described in the Introduction. A d.c. current was used for the resistivity measurements which were carried out at room temperature up to  $H = 9$  kOe. The MR ratio at a magnetic field  $H$  was defined with the formula  $MR(H) = [R(H) - R_0]/R_0$  where  $R(H)$  is the resistance in an external magnetic field  $H$  and  $R_0$  is the resistance maximum/minimum close to zero magnetic field.

### 3 Magnetoresistance of bulk and nanocrystalline Ni

#### 3.1 Bulk (microcrystalline) Ni

Figure 1 shows the  $MR(H)$  curves for one of the bulk Ni samples of the present study for both the LMR and TMR measurement configurations. The results are in qualitative agreement with the well-known  $MR(H)$  curves reported for bulk Ni [8, 16]. The other two bulk Ni foils investigated exhibited  $MR(H)$  curves very similar to those shown in Fig. 1.

The low-field sections (below about 2–3 kOe) of the  $MR(H)$  curves in Fig. 1 reflect the magnetization process [8, 9] with its field evolution depending on the sample shape, magnetic anisotropy, stresses, etc. Therefore, the  $MR(H)$  curves of individual bulk Ni samples may differ from each other below the external field corresponding to the magnetic saturation. However, above magnetic saturation (i.e., in the single-domain state), the magnetoresistance

also achieves saturation and this manifests itself in a nearly linear variation of the resistivity in this field range [12, 13] which will be discussed later.

The inset in Fig. 1 shows a magnified view of the measured data around  $H = 0$ . We can observe that a sufficient number of data points were measured around the resistance maxima and minima close to zero magnetic field, approximately at the corresponding coercive fields, ensuring that we could capture the true maximum and minimum resistance values. This is important since the maximum/minimum resistance values corresponding to the optimally demagnetized state of the samples serve as the normalization values for the resistance and their accurate knowledge is necessary to get the correct values for the AMR. It should be stressed that having not enough data around  $H = 0$ , one may miss the true resistance maximum/minimum, leading to a smaller AMR value than the true one.

In the saturated (single-domain) state at room temperature, the resistivity depends only on the relative orientation of the magnetization and measuring current [8–13]. For the LMR configuration (magnetization and current are parallel), the resistivity is maximum and for the TMR configuration (magnetization and current are perpendicular to each other), the resistivity is minimum. The difference between the LMR and TMR components in the saturation region defines the AMR [8–13]. The origin of the difference between the LMR and TMR components is the different conduction electron scattering cross-section that is larger for the parallel than for the perpendicular configuration of current flow and magnetization [9–11].

The reduction of the resistivity with increasing magnetic field in the saturation region is due to the gradual suppression of the magnon contribution to the resistivity [7, 9, 13, 17, 18]. This contribution arises from the scattering of conduction electrons on the thermally induced spin-disorder (magnons) at finite temperatures (the magnon suppression is often termed also as paraprocess [18]). In the relatively low magnetic fields investigated here, the magnon suppression contribution can be considered as nearly linearly varying with magnetic field at room temperature [13].

The evaluation of the MR( $H$ ) data was, therefore, performed by fitting a straight line to the data in the saturation region ( $|H| \geq 3$  kOe) [12, 13]. The measured magnetoresistance data for  $|H| \geq 3$  kOe were fitted to the function  $XMR(H) = XMR_s + mH$  where  $X = L$  or  $T$  and  $m < 0$  is the slope of the field dependence in the saturation region and characterizes the magnon suppression term. From the longitudinal ( $LMR_s$ ) and transverse ( $TMR_s$ ) saturation components of the magnetoresistance, the AMR ratio was obtained as  $AMR = LMR_s - TMR_s$ . The resistivity anisotropy splitting  $\Delta\rho_{AMR}$  was obtained as the product of the AMR ratio and the zero-field resistivity  $\rho_0$ .

The values of these parameters for the bulk (microcrystalline) Ni samples as obtained in the present work are given in Table 1. The data given represent averages over several strips and measurements for a given sample as indicated in the first column of Table 1. Our AMR values for the bulk Ni samples Ni #B5 and #GF-Ni(50  $\mu$ m) agree with each other very well whereas the AMR value for the #Ni(99.99+ %) sample is slightly higher by about a factor of 1.11. As noted before, there was no Co or Fe contamination in the third sample that could cause a measurable increase of the AMR ratio. Thus, at the moment we do not have an explanation for the slightly higher AMR ratio of the third sample.

Table 1 lists also all previously reported AMR data for bulk Ni metal [16, 19–25]. Unfortunately, not much structural and impurity information is available about most of the samples used in these earlier studies. The two AMR values above 3% [16, 19] may originate, e.g., from Co impurities in the Ni samples investigated since it is known [12] that the addition of a few percent of Co can increase the AMR of Ni metal to this extent. Some of the other data are close to our AMR values, but most of them are smaller and scattered around 2%. The

**Table 1** Room-temperature electrical transport parameters of the  $\mu\text{-c-Ni}$  foils investigated, together with relevant literature data on bulk Ni metal

Samples of this work	AMR ratio (%)	$m$ (%/kOe)	$\rho_0$ ( $\mu\Omega\text{-cm}$ )	$\Delta\rho_{\text{AMR}}$ ( $\mu\Omega\text{-cm}$ )
Ni #B5 (7 strips, 11 measurements)	+ 2.39 (16)	− 0.0185 (180)	7.36 (22) [6]	+ 0.176 (12)
#GF-Ni(50 $\mu\text{m}$ ) (2 strips, 6 measurements)	+ 2.43 (14)	− 0.0174 (90)	7.32 (22) [6]	+ 0.177 (10)
#Ni(99.99+ %) (2 strips, 8 measurements)	+ 2.67 (13)	− 0.0167 (90)	7.54 (22) [6]	+ 0.201 (10)
Literature data				
Jones and Malam [19]	+ 3.15	− 0.0040 (L) − 0.0324 (T)		
Alocco [20]	+ 2.30	$\sim 0$		
Englert [16]	+ 3.03	− 0.0373 (L) − 0.0206 (T)		
Heaps [21] ED Ni	+ 2.50	− 0.0060 (L) − 0.0120 (T)		
McGuire [9, 22] [Ni (0.58 at.% Co)]	+ 2.02	− 0.0200	7.8	+ 0.16
Kaul [23]	+ 1.80			
Jayaraman and Pal [24]	+ 1.97		7.77	+ 0.153
Inagaki et al. [25]	+ 2.16			
Raquet et al. [18]		− 0.0280 (140)		

The measured magnetoresistance data for  $|H| \geq 3$  kOe were fitted to the function  $XMR(H) = XMR_s + mH$  where  $X = L$  or  $T$  and  $m < 0$ . From the saturation longitudinal ( $LMR_s$ ) and transverse ( $TMR_s$ ) components of the magnetoresistance, the AMR ratio was obtained as  $AMR = LMR_s - TMR_s$ . The resistivity anisotropy splitting  $\Delta\rho_{\text{AMR}}$  was obtained as the product of the AMR ratio and the zero-field resistivity  $\rho_0$ . The figures in brackets after the data represent the scatter to cover all measured data for the given parameter

smaller AMR values in comparison with ours may have resulted, e.g., from missing the true maxima/minima of  $R$  around  $H = 0$  as discussed above.

It is useful to quote the room-temperature value of  $\Delta\rho_{\text{AMR}}$  which is the resistivity anisotropy splitting between the longitudinal and transverse configurations in the saturation region ( $\Delta\rho_{\text{AMR}} = \rho_{\text{LMR}_s} - \rho_{\text{TMR}_s}$ ) and can be conveniently obtained as the product of the zero-field resistivity and the AMR ratio. When measuring the magnetoresistance of ferromagnets, in most cases only the AMR ratio is determined since it can be measured with relatively large accuracy without the need of knowing the precise sample dimension parameters. As demonstrated in Ref. [6], our resistivity measurement accuracy is about 3% and so we can get the  $\Delta\rho_{\text{AMR}}$  data given in Table 1 with the same accuracy. There are relatively few  $\Delta\rho_{\text{AMR}}$  data for bulk Ni [9, 24] and these are shown also in Table 1; corresponding to the smaller AMR for these samples, the reported  $\Delta\rho_{\text{AMR}}$  values are also smaller than our values.

The second column in Table 1 gives the high-field slope  $m$  of the  $MR(H)$  curves. It is noted that whereas the AMR ratio could be determined for a given sample with reasonable reproducibility (within less than 10% of the average), the experience with the current magnetotransport workstation was that the magnon-suppression term characterized by the

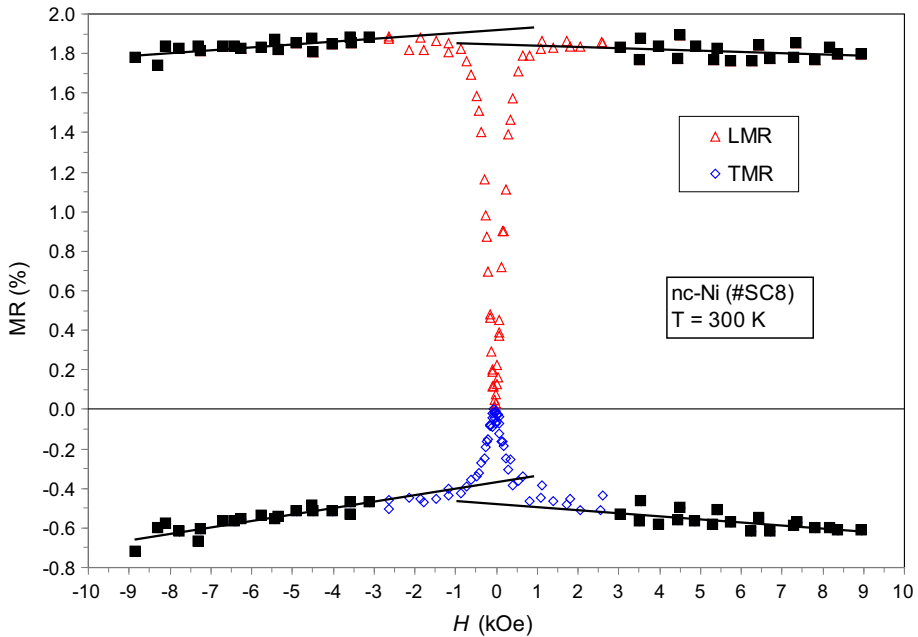


**Fig. 2** Room-temperature longitudinal (LMR) and transverse (TMR)  $MR(H)$  curves for the nc-Ni sample with the smallest grain size. The solid squares over the high-field ( $|H| \geq 3$  kOe) data points indicate data used for a linear fitting and the fit is also indicated (thick solid line)

high-field slope  $m$  of the  $MR(H)$  curves could not be established accurately. Our  $m$  values were very scattered and for a given sample, we often obtained  $m$  values differing by a factor of 2 or 3 in consecutive measurements. The same large scatter can be observed also for the literature data summarized in Table 1. Nevertheless, according to the data listed in Table 1, the average  $m$  value for bulk Ni can be in the range  $-0.0100\%/kOe < m < -0.0300\%/kOe$ . To determine  $m$  with sufficient accuracy for the present bulk Ni foils having a thickness of typically  $50 \mu\text{m}$ , we need to improve the electronic stability of our measurement setup by at least an order of magnitude.

### 3.2 Nanocrystalline Ni

The  $MR(H)$  curves of all nc-Ni foil samples were qualitatively very similar to those of the bulk Ni samples (see Sect. 3.1). The measured  $MR(H)$  curves for the nc-Ni sample with the highest resistivity (smallest grain size) [6] is shown in Fig. 2.

The evaluation of the  $MR(H)$  curves of the nc-Ni samples proceeded in the same manner as for the bulk Ni samples in Sect. 3.1. The results are summarized in Table 2. Included are here also the  $\Delta\rho_{AMR}$  values (column 5) obtained with the help of the resistivity data reported on the same samples in Ref. [6] and reproduced in column 4 together with their grain sizes in column 6. We have also listed relevant literature data for Ni thin films [26–29] which are presumably also nanocrystalline.

The AMR data of the ED Ni series samples are displayed in Fig. 3 as a function of the grain size of the same samples taken from Ref. [6]. The AMR values are scattered between  $+2.2$  and  $+2.5\%$  for the nc-Ni samples free of Co impurity and no obvious trend can be

**Table 2** Room-temperature electrical transport parameters of the electrodeposited nc-Ni foils investigated, together with reported Ni thin film data

Samples in this work (no Co) (codes from Ref. [6])	AMR ratio (%)	$m$ (%/kOe)	$\rho_0$ ( $\mu\Omega\text{-cm}$ )	$\Delta\rho_{\text{AMR}}$ ( $\mu\Omega\text{-cm}$ )	TEM grain size (nm) [6]
#SC7	+ 2.45	− 0.0111	11.71 [6]	+ 0.287	29 ± 2
#SC8	+ 2.31	− 0.0171	11.70 [6]	+ 0.270	29 ± 4
#NC2	+ 2.44	− 0.0077	10.46 [6]	+ 0.255	33 ± 4
#NC10	+ 2.28	− 0.0264	9.91 [6]	+ 0.226	40 ± 16
#FA3	+ 2.54	− 0.0183	11.01 [6]	+ 0.280	66 ± 9
#TN3	+ 2.18	− 0.0143	9.81 [6]	+ 0.214	105 ± 13
#NA5	+ 2.37	− 0.0218	8.83 [6]	+ 0.209	93 ± 18
#NA6	+ 2.55	− 0.0074	8.88 [6]	+ 0.226	86 ± 15
#B2	+ 1.88	− 0.0134	8.78 [6]	+ 0.165	
#Ni(TKE)	+ 2.04	− 0.0099	9.96 [6]	+ 0.203	
Samples in this work (with Co) (codes from Ref. [6])					
#TN2 (2.9 at.% Co)	+ 3.32	− 0.0299	9.77 [6]	+ 0.324	79 ± 8
#NC*33 (3.6 at.% Co)	+ 4.32	− 0.0304	8.52 [6]	+ 0.368	148 ± 33
Literature data on Ni thin films					
Asama et al. [26]	+ 1.4		10.7	+ 0.15	
Galepov [27]	+ 1.18		11	+ 0.13	
McGuire et al. [28]	+ 2.21		12.1	+ 0.267	
Myung and Nobe [29]	+ 2.40		9	+ 0.216	
Madduri and Kaul [7]		− 0.0180 (90) (between 10 and 20 kOe)			

The measured magnetoresistance data for  $|H| \geq 3$  kOe were fitted to the function  $XMR(H) = XMR_s + m H$  where  $X = L$  or  $T$  and  $m < 0$ . From the saturation longitudinal ( $LMR_s$ ) and transverse ( $TMR_s$ ) components of the magnetoresistance, the AMR ratio was obtained as  $AMR = LMR_s - TMR_s$ . The resistivity anisotropy splitting  $\Delta\rho_{\text{AMR}}$  was obtained as the product of the AMR ratio and the zero-field resistivity  $\rho_0$

observed from these data. On the other hand, the two nc-Ni(Co) samples with a small amount of Co impurity (about 3 at.%) have significantly larger AMR values, and the observed AMR increase is in good quantitative agreement with the reported influence of Co on the AMR of Ni metal at low Co concentrations [12].

The  $m$  values are given in column 3 of Table 2. These data could be obtained with better accuracy here than for the bulk Ni foils since the nc-Ni foils had a typical thickness of 20  $\mu\text{m}$  or even less. The  $m$  values for the pure nc-Ni samples are typically between  $-0.0100$  and  $-0.0200\%/k\text{Oe}$  and very similar values were obtained also by Madduri and Kaul [7] for their ED nc-Ni samples. By looking at the data given above for the bulk Ni samples (Table 1), we can also establish that the microstructural differences between bulk ( $\mu\text{c}$ ) and nc-Ni

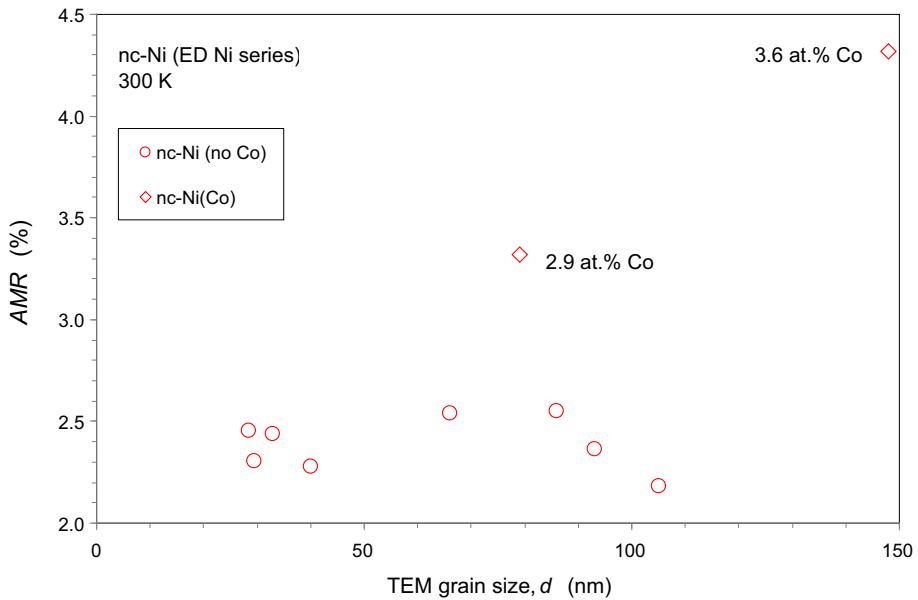


**Fig. 3** AMR data as a function of the grain size for the present nc-Ni and nc-Ni(Co) samples

do not result in a noticeable change of the magnon suppression term which can actually be expected.

An analysis of the magnetotransport parameters of the nc-Ni samples will be attempted in Sect. 4 where we will look for a correlation between the zero-field resistivity and the  $\Delta\rho_{\text{AMR}}$  values of the corresponding samples.

#### 4 Correlation of $\Delta\rho_{\text{AMR}}$ with the zero-field resistivity $\rho_0$

The available present and literature room-temperature data for  $\Delta\rho_{\text{AMR}}$  and for the zero-field resistivity,  $\rho_0$ , of Ni metal are displayed against each other in Fig. 4. It can be seen that the larger the zero-field resistivity, the larger the quantity  $\Delta\rho_{\text{AMR}}$ . The data of Co-free nc-Ni samples from the ED Ni series can be fitted to a straight line going through the origin and the slope of the line yields  $\text{AMR} = +2.39\%$ . (It is noted that the fit was performed by forcing the fit line to go through the origin and the fit quality was  $R^2 = 0.8196$ . Performing the fit in a manner that the ordinate intercept was a free variable, the result was  $\Delta\rho_{\text{AMR}} = 0.0246 \rho_0 - 0.0075$  with a fit quality  $R^2 = 0.8203$  and the position of the fit line over the data points was hardly different from the forced-fit line going through the origin. Since the fit quality was practically the same in both cases and the slopes differed by some 3% only, we can rely on the forced fit result which corresponds to physical expectation in that if the resistivity is zero, no anisotropic splitting can occur).

The other two investigated Co-free ED Ni samples which were prepared under different conditions as those of the ED Ni series yielded data points below the fitted line. As to the (probably also nanocrystalline) Ni thin film data, two of them are in good agreement with the results for the current Co-free ED Ni series whereas the other two data deviate markedly

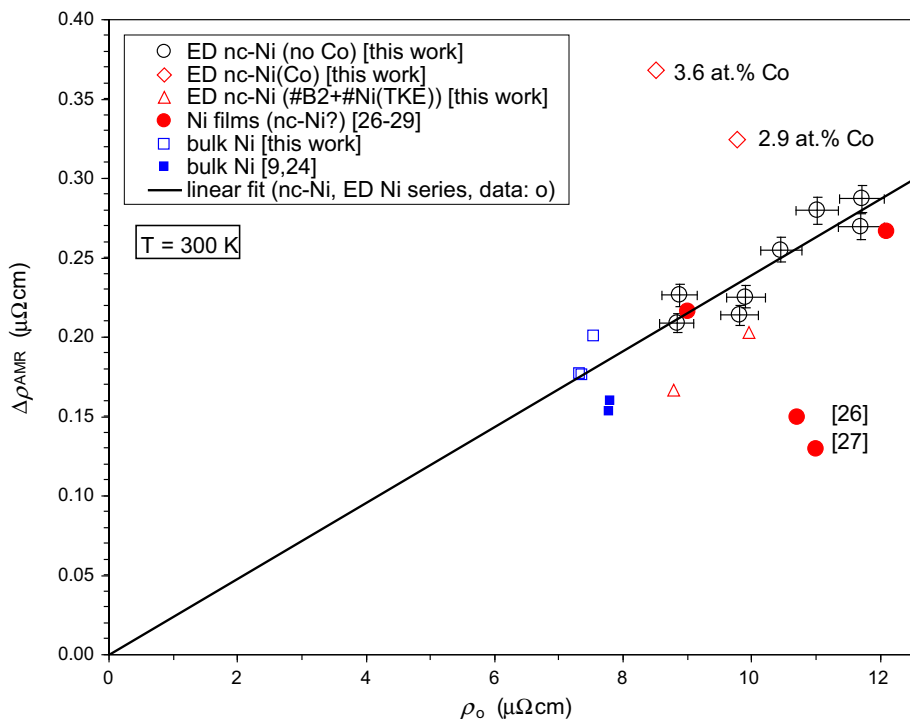


**Fig. 4** Correlation of  $\Delta\rho_{\text{AMR}}$  with the zero-field resistivity  $\rho_0$  at room temperature for bulk ( $\mu\text{c}$ ) and nc-Ni metal. The solid line corresponds to a linear fit with  $\Delta\rho_{\text{AMR}} = 0.0239 \rho_0$  (fit quality:  $R^2 = 0.8196$ ) to the data of the Co-free nc-Ni samples of the present ED Ni series (circle) for which the  $\pm 3\%$  error bars mentioned in the text are also indicated. The two nc-Ni samples with Co impurity (diamond) are displayed with different symbols and, similarly, also the two other ED nc-Ni samples prepared earlier under different conditions (triangle). Our bulk ( $\mu\text{c}$ ) Ni results are indicated by the open squares (square). Several literature data are also included (see the legend) for (probably nc) Ni film samples (filled circle) and for bulk Ni samples (filled square)

form the common trend. The nc-Ni(Co) samples clearly deviate from the trend indicated by the fit line and the presence of Co is responsible for this.

It can be observed that the  $\Delta\rho_{\text{AMR}}$  values for two of the bulk Ni samples (Ni #B5 and #GF-Ni(50  $\mu\text{m}$ )) lie very close to the fitted line, in agreement with their similar AMR values (2.39% and 2.43%, respectively, see Table 1). The data for the third bulk Ni sample of the present work (#Ni(99.99+ %)) and two literature data are slightly further apart from, but still fairly close to the fit line.

Of course, not surprisingly, the average of the AMR values in Table 1 (and shown also in Fig. 3) for the pure (Co-free) nc-Ni samples agrees exactly with the AMR = + 2.39% value derived from the slope of the straight line in Fig. 4. However, displaying the magnetoresistance data in the form of Fig. 4 underpins that the apparent scatter of the AMR data in Fig. 3 is not of random nature, but rather governed by the zero-field resistivity of the individual nc-Ni samples.

The majority of the data included in Fig. 4 demonstrate that in pure Ni metal the anisotropy splitting of the longitudinal and transverse magnetoresistance components in the magnetically saturated state as measured by the quantity  $\Delta\rho_{\text{AMR}}$  is clearly proportional to the absolute value

of the zero-field resistivity. This proportionality is apparently independent of the microstructural features of the Ni samples and is an inherent characteristic of Ni metal, reflecting the anisotropy of electron scattering as far as the electron flow direction with respect to the local magnetic moment orientation is concerned (parallel or perpendicular).

At room temperature, the dominant contribution to the resistivity of bulk Ni metal is due to the electron–phonon and, to a less extent, the electron–magnon interaction [7]. In the case of the pure (i.e., Co-free) nc-Ni samples, we were able to induce an increase in the zero-field resistivity by introducing a large amount of grain boundaries representing additional scattering centers for the conduction electrons. On the other hand, the electron scattering processes causing the spontaneous anisotropy of the resistivity (i.e., the AMR) depend on the electronic band structure of the metal matrix. The linear relation between  $\Delta\rho_{\text{AMR}}$  and  $\rho_0$  in Fig. 4 may suggest that we could increase here the resistivity without noticeably modifying the overall electronic density of states (DOS) around the Fermi level since the resistivity anisotropy increased only in proportion to the enhancement of the resistivity itself.

According to the following considerations, we can make an estimate to what extent the Fermi level DOS remains unchanged in our nc-Ni samples with respect to bulk Ni. The smallest grain size was around 30 nm (see Table 2). Palumbo et al. [30] estimated that at this grain size about 10% of the atoms are in the grain boundaries whereas the fraction of atoms in triple line junctions is negligible here. They assumed a grain boundary width of 1 nm and the modeling results of Derlet et al. [31] for nc-Ni indicated that the width can actually be even smaller, depending on the way of defining the grain boundary width. For the largest grains sizes in our samples (around 100 nm), the grain boundary atomic fraction drops down to about 3%. Furthermore, Crampin et al. [32] has carried out a detailed calculation of the local electronic DOS for several atomic layers near the core of a (210) tilt boundary in nickel. It is generally known that any deviation from structural perfectness leads to a smearing out of the fine peaks of DOS curve which latter reflect the details of the crystal symmetry of the given metal. Since only electrons around the Fermi level can participate in the conduction process, the DOS at the Fermi level is of interest only for us currently. Bulk Ni metal itself has a steep flank of the DOS at the Fermi level. Crampin et al. [32] has found that there is indeed a smearing out of the DOS peaks for atomic layers close to the core of the grain boundary and bandwidth reduction also appears here. On the other hand, they could also demonstrate that the bandwidth is fully restored already for layer 3 and for this layer the DOS flank at the Fermi level is already indistinguishable from bulk Ni. If we take now into account that layer 3 in their model consists of atoms which are actually first neighbors to atoms of the grain boundary core (defined as layer 0), we can come to the conclusion that the width of the grain boundary over which the atoms have a Fermi level DOS different from that of bulk Ni is below even a half of a nanometer. Thus, the fraction of atoms with different DOS than bulk Ni are indeed very small and we can assume that in our samples the overall DOS at the Fermi level may not differ significantly from that of bulk Ni. In this manner, in the grain size range investigated, nc-Ni can be considered as behaving like bulk Ni from the viewpoint of the spontaneous anisotropy of the resistivity and we can expect the linear relation between  $\Delta\rho_{\text{AMR}}$  and  $\rho_0$  as observed in Fig. 4.

The distinctly deviating  $\Delta\rho_{\text{AMR}}$  values for the Ni samples with a small Co-content further underpin that the observed linear behavior derives from the electronic structure of the pure Ni metal matrix since adding a small amount of Co to Ni changes slightly the matrix electronic structure in a manner that a larger resistivity anisotropy splitting  $\Delta\rho_{\text{AMR}}$  arises.

Evidently, another means of resistivity modification without substantially altering the Fermi level DOS of the metal matrix is a change of the temperature of the metal, either in the bulk ( $\mu\text{c}$ ) or nc state. According to the note of Campbell and Fert [10], the AMR ratio is

fairly independent of the temperature. This actually corresponds to the statement that for a given metal matrix,  $\Delta\rho_{\text{AMR}}$  is proportional to the zero-field resistivity if the temperature is used as an internal parameter.

Along this line, our next step is to study the correlation of  $\Delta\rho_{\text{AMR}}$  and the zero-field resistivity for both bulk ( $\mu\text{c}$ ) and nc Ni metal below room temperature. It can be expected that the data should fall for both structural states on the straight line of Fig. 4 of the present work.

## 5 Summary

In this work, the room-temperature magnetoresistance (MR) characteristics of nc-Ni metal with various grain sizes (between 30 and 100 nm) were investigated for the first time. The  $\text{MR}(H)$  curves were measured to determine the AMR ratio and the results were analyzed together with corresponding data measured on bulk (microcrystalline) Ni metal samples. The magnitude of the AMR ratio was found to be in the range from about 2 to 2.5% for both bulk Ni and nc-Ni and did not show a systematic dependence on the grain size. On the other hand, the field-induced resistivity anisotropy splitting  $\Delta\rho_{\text{AMR}}$  in the magnetically saturated state was found to be proportional to the zero-field resistivity of the same samples with different grain sizes. The slope of this proportionality relation provided an AMR ratio of 2.4% for polycrystalline Ni metal which seems to be fairly independent of the microstructural features (coarse grained or nanocrystalline).

Thus, the present room-temperature magnetoresistance results demonstrated that the resistivity anisotropy splitting  $\Delta\rho_{\text{AMR}}$  is proportional to the zero-field resistivity of the metal matrix in the sense that if we can change the resistivity of the matrix without changing noticeably the electronic density of states of the metal matrix, at least around the Fermi level, then the induced change of  $\Delta\rho_{\text{AMR}}$  will be proportional to the resistivity change. The proportionality factor, which is actually the AMR ratio, is an inherent characteristic of the metal matrix.

**Acknowledgements** Open access funding provided by MTA Wigner Research Centre for Physics (MTA Wigner FK, MTA EK). Work supported by the Research Group Linkage Programme (Project Ref. 3.4-1001292-HUN-IP) of the Alexander von Humboldt Foundation, Germany with the funding provided by the Federal Ministry of Education and Research, Germany. A critical reading of the manuscript by H. Ebert is gratefully acknowledged.

**Open Access** This article is licensed under a Creative Commons Attribution 4.0 International License, which permits use, sharing, adaptation, distribution and reproduction in any medium or format, as long as you give appropriate credit to the original author(s) and the source, provide a link to the Creative Commons licence, and indicate if changes were made. The images or other third party material in this article are included in the article's Creative Commons licence, unless indicated otherwise in a credit line to the material. If material is not included in the article's Creative Commons licence and your intended use is not permitted by statutory regulation or exceeds the permitted use, you will need to obtain permission directly from the copyright holder. To view a copy of this licence, visit <http://creativecommons.org/licenses/by/4.0/>.

## References

1. G. Binasch, P. Grünberg, F. Saurenbach, W. Zinn, *Phys. Rev. B* **39**, 4828 (1989)
2. M.N. Baibich, J.M. Broto, A. Fert, F. Nguyen Van Dau, F. Petroff, P. Etienne, G. Creuzet, A. Friederich, J. Chazelas, *Phys. Rev. Lett.* **61**, 2472 (1988)
3. V.V. Kruglyak, S.O. Demokritov, D. Grundler, *J. Phys. D Appl. Phys.* **43**, 264001 (2010)

4. M. Krawczyk, D. Grundler, *J. Phys. Condens. Matter* **26**, 123202 (2014)
5. J.M. Ziman, *Electrons and phonons, VI* (Clarendon Press, Oxford, 1960)
6. I. Bakonyi, V.A. Isnaini, T. Kolonits, Z. Czigány, J. Gubicza, L.K. Varga, E. Tóth-Kádár, L. Pogány, L. Péter, H. Ebert, *Philos. Mag.* **99**, 1139 (2019). <https://doi.org/10.1080/14786435.2019.1580399>
7. P.V.P. Madduri, S.N. Kaul, *Phys. Rev. B* **95**, 184402 (2017)
8. R.M. Bozorth, *Ferromagnetism* (Van Nostrand, New York, 1951)
9. T.R. McGuire, R.I. Potter, *IEEE Trans. Magn.* **11**, 1018 (1975)
10. I.A. Campbell, A. Fert, in *Transport Properties of Ferromagnets*, ed. E.P. Wohlfarth. Ferromagnetic materials, vol. 3 (North-Holland, Amsterdam, 1982)
11. R.C. O'Handley, *Modern magnetic materials principles and applications* (Wiley-Interscience, New York, 2000)
12. B.G. Tóth, L. Péter, Á. Révész, J. Pádár, I. Bakonyi, *Eur. Phys. J. B* **75**, 167 (2010)
13. I. Bakonyi, *Eur. Phys. J. Plus* **133**, 521 (2018)
14. T. Kolonits, P. Jenei, B.G. Tóth, Z. Czigány, J. Gubicza, L. Péter, I. Bakonyi, *J. Electrochem. Soc.* **163**, D107 (2016)
15. T. Kolonits, P. Jenei, L. Péter, I. Bakonyi, Zs Czigány, J. Gubicza, *Surf. Coat. Technol.* **349**, 611–621 (2018)
16. E. Englert, *Ann. Phys.* **14**, 589 (1932)
17. B. Raquet, M. Viret, J.M. Broto, E. Sondergard, O. Cespedes, R. Mamy, *J. Appl. Phys.* **91**, 8129 (2002)
18. B. Raquet, M. Viret, E. Sondergard, O. Cespedes, R. Mamy, *Phys. Rev. B* **66**, 024433 (2002)
19. W. Jones, J.E. Malam, *Philos. Mag.* **27**, 649 (1914)
20. G. Alocco, *Nuovo Cim.* **10**, 153 (1932)
21. C.W. Heaps, *Phys. Rev.* **55**, 1069 (1939)
22. T.R. McGuire, *AIP Conf. Proc.* **24**, 435 (1975)
23. S.N. Kaul, *J. Phys. F* **7**, 2091 (1977)
24. V. Jayaraman, B. Pal, *Indian J. Phys.* **52A**, 411 (1978)
25. M. Inagaki, M. Suzuki, Y. Iwama, U. Mizutani, *Jpn. J. Appl. Phys.* **25**, 1514 (1986)
26. K. Asama, K. Takahasi, M. Hirano, *AIP Conf. Proc.* **18**, 110 (1973)
27. P.S. Galepov, *Izv. VUZ Fizika* **9**, 64 (1974)
28. T.R. McGuire, J.A. Aboaf, E. Klokhholm, *IEEE. Trans. Magn.* **20**, 972 (1984)
29. N.V. Myung, K. Nobe, *J. Electrochem. Soc.* **148**, C136 (2001)
30. G. Palumbo, S.J. Thorpe, K.T. Aust, *Scripta Met. Mater.* **24**, 1347 (1990)
31. P.M. Derlet, S. Van Petegem, H. Van Swygenhoven, *Phys. Rev. B* **71**, 024114 (2005)
32. S. Crampin, D.D. Vvedensky, J.M. MacLaren, M.E. Eberhart, *Phys. Rev. B* **40**, 3413 (1989)